Computers and Structures 244 (2021) 106429

Contents lists available at ScienceDirect

Computers and Structures

journal homepage: www.elsevier.com/locate/compstruc

On the convergence of overlapping elements and overlapping meshes

Junbin Huang, Klaus-Jürgen Bathe *

Department of Mechanical Engineering, Massachusetts Institute of Technology, Cambridge, MA 02139, USA

ARTICLE INFO

Article history:
Received 13 August 2020
Accepted 21 October 2020

Keywords:
Finite elements
Overlapping elements
Overlapping meshes
Meshing
AMORE paradigm
Convergence

ABSTRACT

Two novel finite element schemes were earlier proposed to reduce the meshing effort needed for practical finite element analysis and their promising performance was demonstrated in the AMORE (AMORE stands for **A**utomatic **M**eshing with **O**verlapping and **R**egular **E**lements) framework. In the first scheme "overlapping finite elements" are established that combine advantages of meshless and traditional finite element methods. A key step is to use polynomial interpolations for the rational shape functions in the meshless method. The scheme enables effective, accurate, and element distortion insensitive numerical solutions. In the second scheme, individual meshes are allowed to overlap quite freely. In our earlier papers we gave illustrative examples and also brief discussions on the convergence of the schemes when used in AMORE. We now focus on presenting deeper insights into the convergence properties through theory and novel illustrative solutions.

1. Introduction

Many numerical algorithms for the solution of partial differential equations have been developed of which finite element methods have, overall, remained by far most prominent for use in engineering and the sciences. However, although abundantly employed, we have not yet harnessed the full potential of finite element methods because a large human effort is usually needed for establishing an effective spatial discretization — the finite element mesh — for the problem to be solved [1].

Our work has focused on the overlapping finite elements to significantly reduce the effort of meshing [2–5]. Overlapping elements were formulated as overlapped regions of polygonal "elements". On each polygonal "element", a local interpolation is established using the method of finite spheres [6], which is a robust meshless method [7], and then these local fields are combined using traditional shape functions. As a result, the overlapping finite element interpolation suffers from much less sensitivity to mesh distortions compared with traditional finite element formulations. An important key step is the interpolation of the rational functions in the method of finite spheres so that the final shape functions are local polynomials. This approach leads to a reduced number of quadrature points. To complement the overlapping element approach, we also proposed a scheme of overlapping meshes. The idea is quite natural: independent meshes are spanned over the domain to be analyzed with these meshes overlapping and together discretizing the complete analysis domain. Any interpolation technique may be used on each mesh. Here the key is to use appropriate weight functions for each mesh since the mesh interpolations are combined using a partition of unity formulation. The implementation requires an algorithm for the triangulation of the overlapped regions for the numerical integration, and we used the plane sweep-based mesh overlay procedure [8,9] to establish the required information.

These new schemes play central roles in the AMORE paradigm. AMORE is a general solution procedure for any CAD or computerized scan representation of physical objects [2–5,10–12]. In the discretization, regular (low-order) traditional finite elements are used to discretize the interior part and the novel overlapping interpolations are used near the boundaries. To reduce the meshing effort, a boundary mesh may either be created using simple rules, e.g. constrained Delaunay triangulation, or be allowed to overlap the interior mesh. In the first case, overlapping elements are effective as they yield a high-order convergence and are insensitive to mesh distortions. In the second case, overlapping meshes are naturally used and the proposed scheme is an effective procedure for coupling the interpolations of the independent meshes.

Of course, allowing "elements" or "cells" to overlap is not a new idea. Successful applications have already been reported in computational fluid mechanics; specifically the so-called Chimera or overset grids were used for finite difference and finite volume methods [13–15]. A corresponding procedure in finite element methods was not proposed as the compatibility requirements have to be satisfied. Researchers therefore worked on alternative approaches to alleviate the meshing issue such as the generalized

* Corresponding author.
E-mail address: kjb@mit.edu (K.J. Bathe).

https://doi.org/10.1016/j.compstruc.2020.106429
0045-7949/

finite element method [16–18], the fictitious domain method [19,20], domain decomposition methods [21], Nitsche's method [22,23], and discontinuous Galerkin methods [24,25]. The generalized finite element method shares some similarities with the fictitious domain method. Indeed, both methods avoid directly meshing the domain by covering the complex domain with a larger, regular mesh. The basic principles however differ. In the generalized finite element method, the variational problem is not changed and the numerical integration is only performed on the physical domain. On the other hand, in the fictitious domain method the governing discretization is derived from an extended variational problem and the original boundary conditions are imposed using Lagrange multipliers. In domain decomposition methods, the original problem is converted into several coupled problems for subdomains, which are usually solved iteratively to yield the solution of the complete problem to be solved. In Nitsche's method non-matching grids are considered and the interface conditions are imposed using the penalty method. In discontinuous Galerkin methods, each element has its own degrees of freedom and the continuity conditions are imposed weakly through the flux.

In engineering applications of finite elements for solids and structures, simple stable procedures with no adjustable penalty coefficients, no Lagrange multipliers, and no numerical stabilization are much preferred [1]. Also, in linear analysis, the governing matrix equations should be symmetric positive definite with a minimum number of equations for reliable and efficient solution using direct sparse solvers. In addition, since traditional finite element methods have been used for many years, a new scheme best retains as many traditional features as possible so that the procedure is user-friendly. Based on these considerations, we proposed the overlapping elements and overlapping meshes for the analysis of solids and structures. Their promising performance suggests that these schemes when used in AMORE provide practical solutions to reducing the effort of meshing.

In this paper, we first briefly review in Section 2 the basic formulations of overlapping elements and overlapping meshes with emphasis on some key points. We only consider two-dimensional analyses but the theory is largely applicable also for three-dimensional solutions. Next, we give in Section 3 a numerical example to illustrate the use of these schemes in the AMORE paradigm. More examples can be found in our previous papers [3–5]. In Section 4, we analyze the convergence rates of these methods. While the ingredients used in these convergence analyses are standard, an interesting and nontrivial case arises when the overlapping of the meshes becomes very thin/small. We give illustrative numerical solutions for this case and establish an error bound for a one-dimensional example. Finally, we present in Section 5 our conclusions and an outlook.

2. Properties of overlapping elements and overlapping meshes

The objective in this section is to briefly review the formulations of overlapping elements and overlapping meshes, with emphasis on key aspects.

2.1. Overlapping elements

Consider a conforming mesh of triangles and quadrilaterals spanning over the analysis domain. The (triangular and quadrilateral) overlapping elements are formulated as the overlapped regions of polygonal "elements", as shown in Fig. 1. Each node is attached to a polygonal "element" formed by all triangles and quadrilaterals sharing the node.

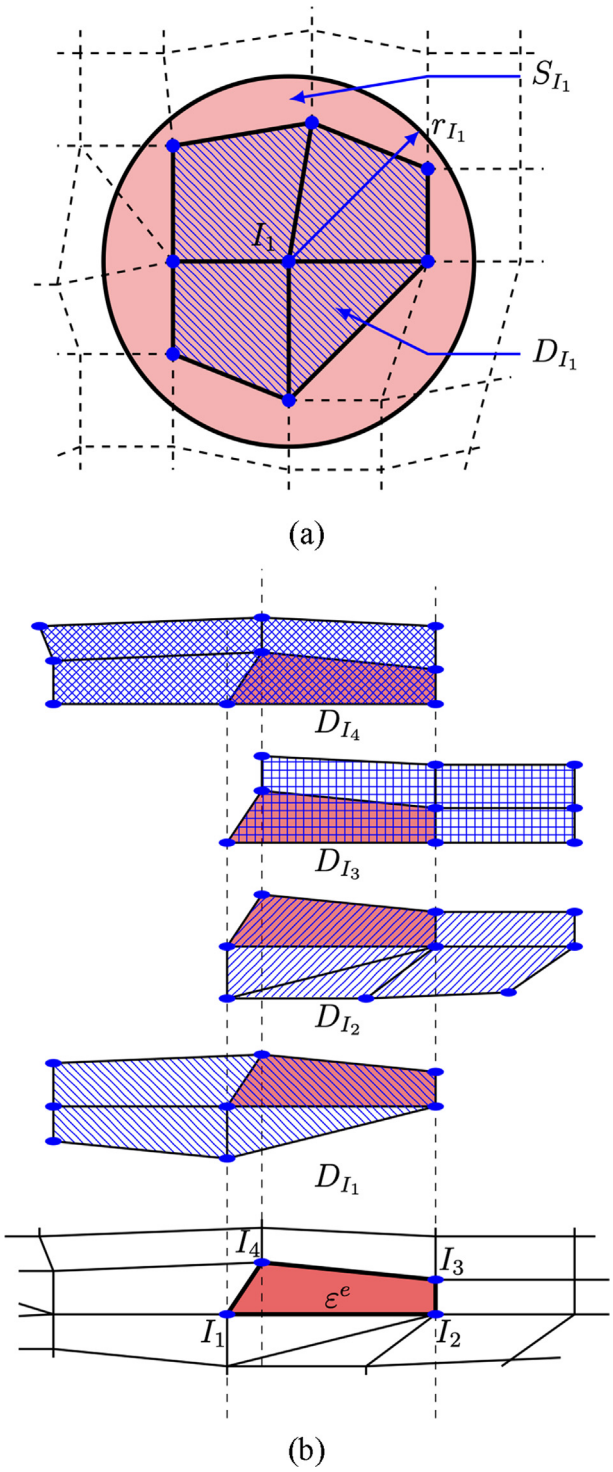

Fig. 1. (a) A typical polygonal "element" D_{I_1} and its local support S_{I_1}. (b) Four polygonal "elements" overlap on the quadrilateral ε^e.

The interpolation (of a scalar function) on a quadrilateral overlapping element is given by

$$u(\boldsymbol{x}) = \sum_{I=1}^{4} h_I(\boldsymbol{x})\psi_I(\boldsymbol{x}), \tag{1}$$

where $h_I(\boldsymbol{x})$ is the traditional shape function for a 4-node finite element, and $\psi_I(\boldsymbol{x})$ is the local interpolation that we establish in the polygonal "element" D_I using the method of finite spheres [6]. Sim-

ilarly, for a triangular overlapping element $u(\boldsymbol{x}) = \sum_{I=1}^{3} h_I(\boldsymbol{x})\psi_I(\boldsymbol{x})$ where we use for the $h_I(\boldsymbol{x})$ the linear shape functions of triangles. We see that the final interpolation is based on a composite scheme drawing on advantages of meshless methods and traditional finite element methods.

The local interpolation can be expressed as

$$\psi_I(\boldsymbol{x}) = \sum_K \phi_K^I(\boldsymbol{x}) \;\; u_K(\boldsymbol{x}), \tag{2}$$

where $\phi_K^I(\boldsymbol{x})$ is the Shepard function and $u_K(\boldsymbol{x})$ is the nodal unknown function. Since Shepard functions are rational functions that for the integration require a large number of quadrature points for a reasonable accuracy, we further interpolate the Shepard functions using high-order isoparametric polynomials. This interpolation is chosen to satisfy the compatibility conditions and reach an effective scheme for overall solution accuracy.

The final interpolations for quadrilateral and triangular overlapping elements are given by

$$\begin{aligned} u(\boldsymbol{x}) &= \textstyle\sum_{I=1}^{4} \rho_I(\boldsymbol{x})\, u_I(\boldsymbol{x}) \quad \text{for quadrilaterals, and} \\ u(\boldsymbol{x}) &= \textstyle\sum_{I=1}^{3} \rho_I(\boldsymbol{x})\, u_I(\boldsymbol{x}) \quad \text{for triangles,} \end{aligned} \tag{3}$$

where $\rho_I(\boldsymbol{x})$ is the new shape function, which is a local polynomial, a cubic function in each of the local coordinates, and $u_I(\boldsymbol{x})$ is the nodal unknown function with to be solved for degrees of freedom. If we use the quadratic basis as the nodal unknown function, we have $u_I(\boldsymbol{x}) = a_{I1} + a_{I2}x + a_{I3}y + a_{I4}x^2 + a_{I5}xy + a_{I6}y^2$. Other suitable functions may also be used as nodal unknown functions, for applications to solve wave propagation problems see [26,27].

The detailed construction of the overlapping interpolations can be found in our previous papers [3,4], where the imposition of boundary conditions and the coupling to traditional finite elements are also discussed. We note that the overlapping elements are used in a finite element program in the same manner as traditional finite elements, but the bandwidth is now larger because of the larger number of degrees of freedom per node. However, each overlapping finite element is more powerful (see Section 4), so that coarser meshes can be used for the analysis and in AMORE the overlapping elements are usually only used near the boundaries of the domain as demonstrated in Section 3.

2.2. Overlapping meshes

Using overlapping meshes, the premise is that for complex geometries, the difficulties of meshing may be overcome by using independent meshes over different parts of the object. These meshes overlap to form a spatial discretization of the complete analysis domain. A schematic description is shown in Fig. 2(a), where a boundary mesh overlaps the interior mesh.

In general, the domain is covered by subdomains that together cover the whole domain, with each subdomain meshed using existing algorithms. The key points of the scheme are then how the interpolation fields of the subdomains are combined and how an effective implementation is established.

Considering as an example the case of Fig. 2(b), the domain Ω is decomposed into three subdomains Ω_i (i = 1, 2, 3). Each subdomain boundary is divided into an interior part Γ_i^*, which is inside the analysis domain, and an exterior part Γ_i. The (regular and quasi-uniform) mesh on Ω_i is denoted by $\mathscr{T}_i$. The shortest distance between the interior boundary of Ω_i and the interior boundary of $\cup_{j\neq i}\Omega_j$ is denoted by h_i^* (see Fig. 2(c) for the example). Let $h^* = \min_i\{h_i^*\}$ considering all i. The maximum element size of $\mathscr{T}_i$ is denoted by h_i.

Assume a continuous local (scalar) approximation $u_i(\boldsymbol{x})$ is constructed on $\mathscr{T}_i$. The final global approximation is expressed as

$$u = \sum_i w_i(\boldsymbol{x})u_i(\boldsymbol{x}), \tag{4}$$

where $w_i(\boldsymbol{x})$ is a continuous, non-negative weight function based on the overlapping of the meshes. To satisfy the polynomial reproducing condition, we must have $\sum_i w_i(\boldsymbol{x}) = 1$ for all points on the analysis domain. In addition, we want the final interpolation to be identical to the local interpolation if an element does not overlap with any other mesh. As a result, each weight function must vanish outside its corresponding subdomain. In the proposed implementation, the weight functions are all piecewise linear functions such that the numerical integration effort is not expensive. We identify the overlapping and non-overlapping elements, after which we triangulate the overlapping regions. On each individual mesh, a local weight function is interpolated and normalized to satisfy the partition of unity property.

Detailed descriptions of the interpolation and the algorithms used are given in our previous paper [5] where the imposition of the boundary conditions and stability conditions are also discussed.

We note that the proposed scheme requires the overlapping meshes to match on the boundary of Ω. In addition, the overlapping size h^* must be strictly positive. Then the weight functions are well-defined and satisfy all the conditions mentioned above. Since each local interpolation is compatible in its subdomain, and each weight function is non-negative, continuous and vanishes outside the corresponding subdomain, the global interpolation is also continuous. Further, we see from the basic requirements of the weight functions that each w_i vanishes on the interior boundary of Ω_i and $w_i = 1$ on the interior boundary of $\cup_{j\neq i}\Omega_j$. We can thus reasonably assume that for any point in Ω_i,

$$\begin{aligned} \left|\frac{\partial w_i}{\partial x}\right| &\leqslant \frac{C}{\min\{h_i, h_i^*\}} \leqslant \frac{C}{\min\{h_i, h^*\}}, \\ \left|\frac{\partial w_i}{\partial y}\right| &\leqslant \frac{C}{\min\{h_i, h_i^*\}} \leqslant \frac{C}{\min\{h_i, h^*\}}, \end{aligned} \tag{5}$$

where h_i is the maximum element size of $\mathscr{T}_i$ and C is a constant. Here the element size h_i enters because the weight functions are interpolated on their own mesh (and then normalized). We assume that h^* is sufficiently large to have $\gamma h_i \leqslant h^*$ for all i, where γ is a positive constant.

3. The use of overlapping elements and overlapping meshes in AMORE

We give here a numerical example to demonstrate the use of overlapping elements and overlapping meshes in the AMORE paradigm. As shown in Fig. 3, a plate is loaded along the inside wall of its hole by a uniform torsion. We solve the problem assuming plane stress conditions (and use consistent units in this and all other analysis results given below).

In Fig. 4(a), regular square 4-node incompatible modes elements are used for the interior domain of the plate, and overlapping elements are employed near the curved boundary. The 4-node incompatible elements (shown in blue) perform well since they are of square geometry [1,28]. The overlapping elements using the quadratic basis (shown in red) can be generated relatively easily because they are not sensitive to element distortions. The green 4-node elements are coupling the non-overlapping and the overlapping elements, see References [3,4] for details.

In Fig. 4(b), we give the overlapping meshes used. For the mesh of the interior of the plate, again 4-node incompatible modes elements are used and for the mesh for the curved boundary near the hole 9-node elements are employed. In Fig. 4(c), we present how the two meshes overlap and how the region of overlapping (blue) is further triangulated merely for the numerical integration (hence the high distortions in this triangulation are of no conse-

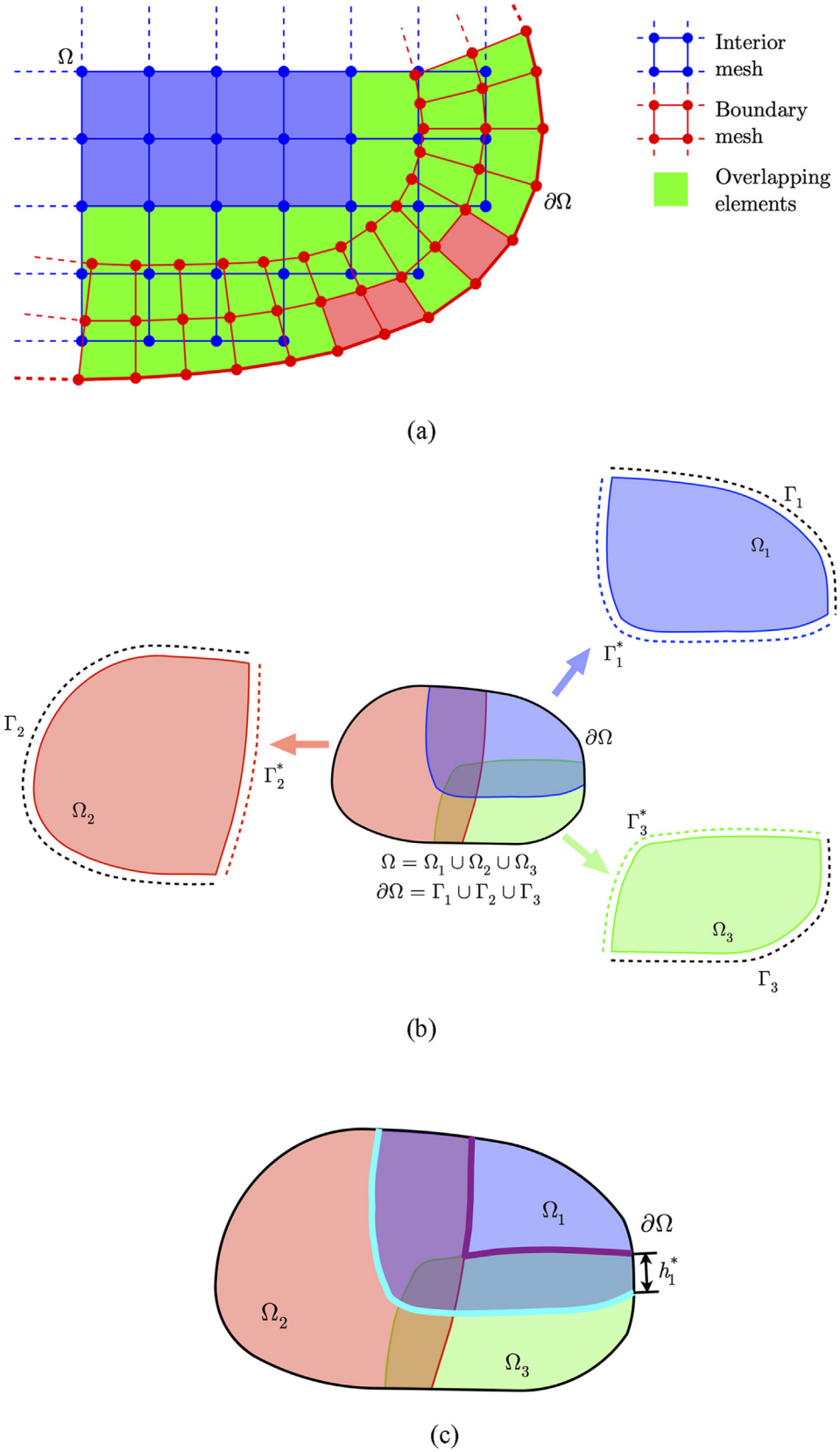

Fig. 2. (a) A boundary mesh overlapping the interior mesh. (b) A typical decomposition into subdomains and the notations for interior boundaries and exterior boundaries. (c) The overlapping size h_1^* is the shortest distance between the interior boundary of the subdomain Ω_1 and the interior boundary of $\Omega_2 \cup \Omega_3$.

quence). The numerical integrations are exact when the overlapping meshes are not distorted [1,5]. If the strain matrices are both from 4-node elements, we use 6 integration points; if the strain matrices are both from 9-node elements, we use 16 points; and if one element is a 4-node element and the other is a 9-node element, we use 12 points.

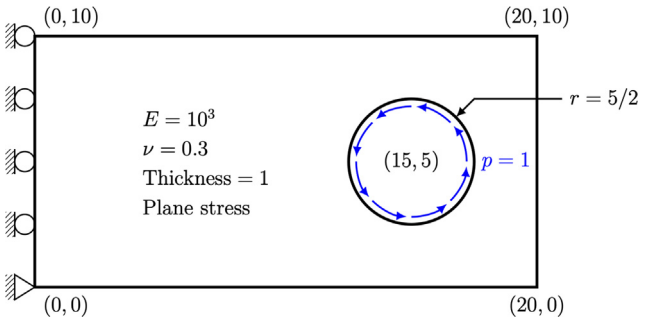

Fig. 3. A plate loaded on its hole.

Finally, in Fig. 4(d), we show the mesh of 4-node incompatible modes elements used in ADINA for a comparison solution.

Some numerical results are listed in Table 1 and plotted in Fig. 5. The reference solutions have been obtained using a very fine 9-node element mesh in ADINA. Overall, the AMORE meshes give very reasonable numerical predictions. We note that the stress results in ADINA are extrapolated from the stresses at the Gauss points and then averaged. The stress results for the overlapping elements are simply averaged at nodes, and could be improved using, for example, the scheme given in Reference [29]. The stress results for the overlapping meshes are non-smoothed, but since high-order elements are used around the hole, the local stress predictions are accurate. To give an indication of the stiffness matrices used, we list the number of degrees of freedom (DOFs) and the number of non-zero sparse matrix entries (NNZ). While, depending on the problem solved, the solution times using the meshes in AMORE may be larger than using a traditional finite element mesh, the savings in hours (or days) used in the meshing of an analysis domain are very desirable.

4. Convergence of methods

Our objective in this section is to discuss the properties of convergence when overlapping elements and overlapping meshes are used.

4.1. Preliminaries

We focus on the solution of a well-posed static problem in two-dimensional linear elasticity. Let Ω be a bounded open connected subset of the plane with a Lipschitz-continuous boundary $\partial\Omega$. Let S_u (displacement boundary) be a subset of $\partial\Omega$ with strictly positive length, and $S_f = \partial\Omega - S_u$ (the force boundary). The stress tensor is denoted by τ_{ij}, and the strain tensor is denoted by ϵ_{ij}. The displacement field $\boldsymbol{u} = (u_1, u_2)$ is the solution of the following system of differential equations:

$$\left.\begin{aligned} &\tau_{ij,j}(\boldsymbol{u}) + f_i = 0 \\ &\tau_{ij}(\boldsymbol{u}) = \lambda\epsilon_{kk}(\mathbf{u})\delta_{ij} + 2\mu\epsilon_{ij}(\mathbf{u}) \\ &\epsilon_{ij}(\mathbf{u}) = \tfrac{1}{2}\left(u_{i,j} + u_{j,i}\right) \end{aligned}\right\}, \tag{6}$$

subject to boundary conditions

$$\left.\begin{aligned} &\boldsymbol{u} = \mathbf{0} \text{ on } S_u \\ &\tau_{ij}(\boldsymbol{u})n_j = g_i \text{ on } S_f \end{aligned}\right\}, \tag{7}$$

where we use the Einstein summation convention, $1 \leqslant i,j \leqslant 2$ are indices, commas in subscripts are used to represent partial derivatives, $\boldsymbol{n} = (n_1, n_2)$ is the unit outer normal of $\partial\Omega$, $\boldsymbol{f} = (f_1, f_2)$ is the body force vector, $\boldsymbol{g} = (g_1, g_2)$ is the vector of boundary tractions, and λ and μ are material constants.

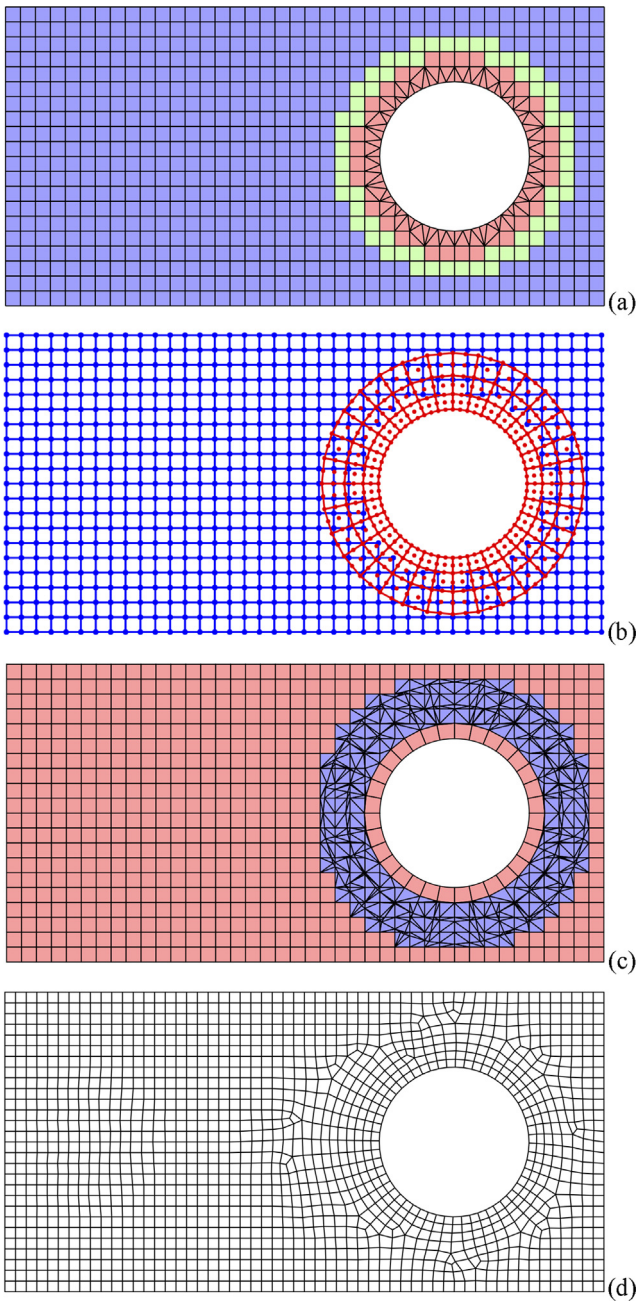

Fig. 4. (a) The AMORE mesh using overlapping elements (red). (b) The AMORE mesh using overlapping meshes. (c) In the overlapping meshes, the red cells correspond to non-overlapping elements and the blue overlapped region is triangulated. (d) The finite element mesh used in ADINA for the results in Table 1. (For interpretation of the references to color in this figure legend, the reader is referred to the web version of this article.)

In the following discussion, $\|\cdot\|_{k,\Omega}$ is the H^k norm over Ω and $|\cdot|_{k,\Omega}$ is the H^k semi-norm over Ω. We simply write $\|\cdot\|_k$ and $|\cdot|_k$ whenever the domain Ω is clearly implied.

The weak solution $\boldsymbol{u} \in \boldsymbol{V}$ of the differential equations satisfies [1]

$$a(\boldsymbol{u}, \boldsymbol{v}) = f(\boldsymbol{v}),\ \forall \boldsymbol{v} \in \boldsymbol{V}, \tag{8}$$

where

$$a(\boldsymbol{u}, \boldsymbol{v}) = \int_\Omega \left\{\lambda u_{i,i} v_{j,j} + 2\mu\epsilon_{ij}(\mathbf{u})\epsilon_{ij}(\mathbf{v})\right\} d\Omega, \tag{9}$$

Table 1
Numerical solutions for the plate problem.

	Overlapping elements	Overlapping meshes	Traditional Finite element mesh	Reference
Energy	0.1784	0.1791	0.1782	0.1794
$u_{\max}$	0.03931	0.03941	0.03929	0.03946
$\tau_{xy\max}$	1.841	1.782	1.766	1.809
$\bar{\tau}_{\max}$	3.572	3.485	3.478	3.508
Number of DOFs	2978	2370	3124	>37,000
NNZ	145,984	86,970	28,301	>610,000

$$f(\boldsymbol{v}) = \int_\Omega \boldsymbol{f}\cdot\boldsymbol{v}\mathrm{d}\Omega + \int_{S_f} \boldsymbol{g}\cdot\boldsymbol{v}\mathrm{d}S, \tag{10}$$

in which we assume $f_i \in L^2(\Omega)$ and $g_i \in L^2(S_f)$ $(i = 1, 2)$, and $\boldsymbol{V} = \{(v_1, v_2) \mid v_i \in H^1(\Omega)$ and $v_i = 0$ on $S_u\}$ is the space of kinematically admissible displacements equipped with the H^1 norm $||\boldsymbol{v}||_1 = \left(\sum_{i=1}^2 ||v_i||_1^2\right)^{1/2}$. The bilinear form $a(\cdot,\cdot)$ is continuous, and also coercive provided the material parameters are reasonable and the displacement constraints are sufficient [1,30–33]. The variational problem (8) then has a unique solution, and also, the energy norm $||\boldsymbol{v}||_e = \sqrt{a(\boldsymbol{v},\boldsymbol{v})}$ is equivalent to the H^1 norm and the H^1 semi-norm $|\boldsymbol{v}|_1 = \left(\sum_{i=1}^2 |v_i|_1^2\right)^{1/2}$.

For the convergence analysis, we assume that the spatial discretization is geometrically exactly representing the domain of analysis. Since the interpolations are continuous, the discretized space $\boldsymbol{V}_h$ is a finite-dimensional subspace of $\boldsymbol{V}$ [1,31–33]. The numerical solution $\boldsymbol{u}_h \in \boldsymbol{V}_h$ then satisfies the variational problem

$$a(\boldsymbol{u}_h, \boldsymbol{v}_h) = f(\boldsymbol{v}_h),\ \forall\ \boldsymbol{v}_h \in \boldsymbol{V}_h. \tag{11}$$

In the following, we ignore the effect of numerical integration and assume that all integrations are exact. In such case, Céa's lemma gives $||\boldsymbol{u} - \boldsymbol{u}_h|| \leqslant C \inf_{\boldsymbol{v}_h\in\boldsymbol{V}_h} ||\boldsymbol{u} - \boldsymbol{v}_h||$ with C a constant determined by the bilinear form [1,31–33], where $||\cdot||$ represents any norm equivalent to the H^1 norm. For simplicity, we only need to consider the approximation error of one displacement component u in the H^1 semi-norm.

4.2. Convergence of overlapping elements

The overlapping elements share many similarities with traditional finite elements. However, the analysis is easier if we view them as special cases of meshless methods. We therefore directly estimate the approximation error in the global coordinate system.

For simplicity, we assume the exact solution u has bounded derivatives up to the order $(k+1)$ where k is the order of nodal basis polynomials. As is usual, we consider a regular and quasi-uniform mesh.

Recall that D_I represents the union of all triangles and quadrilaterals coupling into the node I. For a point $\boldsymbol{x}$ in the polygonal "element" D_I, the line segment from node I to point $\boldsymbol{x}$ is contained in the analysis domain. The Taylor series expansion along this line then allows us to find a local polynomial approximation u_I^* of order k such that

$$\left.\begin{aligned} &|u(\boldsymbol{x}) - u_I^*(\boldsymbol{x})| \leqslant C r_I^{k+1} \\ &\left|\frac{\partial[u(\boldsymbol{x}) - u_I^*(\boldsymbol{x})]}{\partial x}\right| \leqslant C r_I^k \\ &\left|\frac{\partial[u(\boldsymbol{x}) - u_I^*(\boldsymbol{x})]}{\partial y}\right| \leqslant C r_I^k \end{aligned}\right\} \tag{12}$$

holds for all $\boldsymbol{x} \in D_I$, where r_I is the support radius for D_I, and C is a generic constant independent of the element size. Here r_I is equivalent to the maximum overlapping element size h.

We reasonably assume in addition that

$$\left.\begin{aligned} &|\rho_I(\boldsymbol{x})| \leqslant C \\ &\left|\frac{\partial\rho_I(\boldsymbol{x})}{\partial x}\right| \leqslant \frac{C}{r_I} \\ &\left|\frac{\partial\rho_I(\boldsymbol{x})}{\partial y}\right| \leqslant \frac{C}{r_I} \end{aligned}\right\} \tag{13}$$

holds for all $\boldsymbol{x} \in D_I$.

Then using $\sum_I \rho_I = 1$, the approximation error of $u^* = \sum_I \rho_I u_I^*$ in the H^1 semi-norm is

$$\begin{aligned} |u - u^*|_1^2 &= \int_\Omega \left\{ \left|\tfrac{\partial}{\partial x}(u - u^*)\right|^2 + \left|\tfrac{\partial}{\partial y}(u - u^*)\right|^2 \right\}\mathrm{d}\Omega \\ &= \int_\Omega \left\{ \left|\tfrac{\partial}{\partial x}\textstyle\sum_I \rho_I(u - u_I^*)\right|^2 + \left|\tfrac{\partial}{\partial y}\textstyle\sum_I \rho_I(u - u_I^*)\right|^2 \right\}\mathrm{d}\Omega. \end{aligned} \tag{14}$$

Using the relations (12) and (13) we thus have

$$|u - u^*|_1^2 \leqslant Ch^{2k}, \tag{15}$$

where C is a constant independent of the maximum overlapping element size h, and we conclude from Céa's lemma that the overlapping elements with the k-th-order basis lead to a convergence rate of k.

A numerical example illustrating the convergence rates was reported in Reference [4].

4.3. Convergence of overlapping meshes

The convergence of traditional elements that do not overlap is well-established; hence our task reduces to estimating the approximation error over the overlapped regions. For this purpose we use the assumption (5).

Let k_i be the order of finite elements in mesh $\mathscr{T}_i$. Assume that the exact solution u satisfies the standard regularity condition $||u||_{\max_i\{k_i+1\},\Omega} \leqslant +\infty$. Each subdomain Ω_i can be divided into an overlapping part $\Omega_{i,\mathrm{o}} = \Omega_i \cap (\cup_{j\neq i}\Omega_j)$ and a non-overlapping part $\Omega_{i,\mathrm{no}} = \Omega_i - \Omega_{i,\mathrm{o}}$. Using the classic interpolation theory [1,31–34], we can find an approximation u_i^* on subdomain Ω_i such that

$$\begin{aligned} &|u - u_i^*|_{1,\Omega_i}^2 = |u - u_i^*|_{1,\Omega_{i,\mathrm{no}}}^2 + |u - u_i^*|_{1,\Omega_{i,\mathrm{o}}}^2 \leqslant Ch_i^{2k_i}, \\ &\|u - u_i^*\|_{0,\Omega_i}^2 = \|u - u_i^*\|_{0,\Omega_{i,\mathrm{no}}}^2 + \|u - u_i^*\|_{0,\Omega_{i,\mathrm{o}}}^2 \leqslant Ch_i^{2k_i+2}, \end{aligned} \tag{16}$$

where C is a generic constant independent of the maximum element size h_i of the mesh.

Taking $u^* = \sum_i w_i u_i^*$ as a global approximation, the approximation error is

$$\begin{aligned} |u - u^*|_{1,\Omega}^2 &= |u - u^*|_{1,\cup_i\Omega_{i,\mathrm{o}}}^2 + \textstyle\sum_i |u - u^*|_{1,\Omega_{i,\mathrm{no}}}^2 \\ &= |u - u^*|_{1,\cup_i\Omega_{i,\mathrm{o}}}^2 + \textstyle\sum_i |u - u_i^*|_{1,\Omega_{i,\mathrm{no}}}^2 \\ &\leqslant |u - u^*|_{1,\cup_i\Omega_{i,\mathrm{o}}}^2 + C\textstyle\sum_i h_i^{2k_i}, \end{aligned} \tag{17}$$

where the first and second terms on the right-hand side represent the errors over the overlapping and the non-overlapping regions, respectively. Also

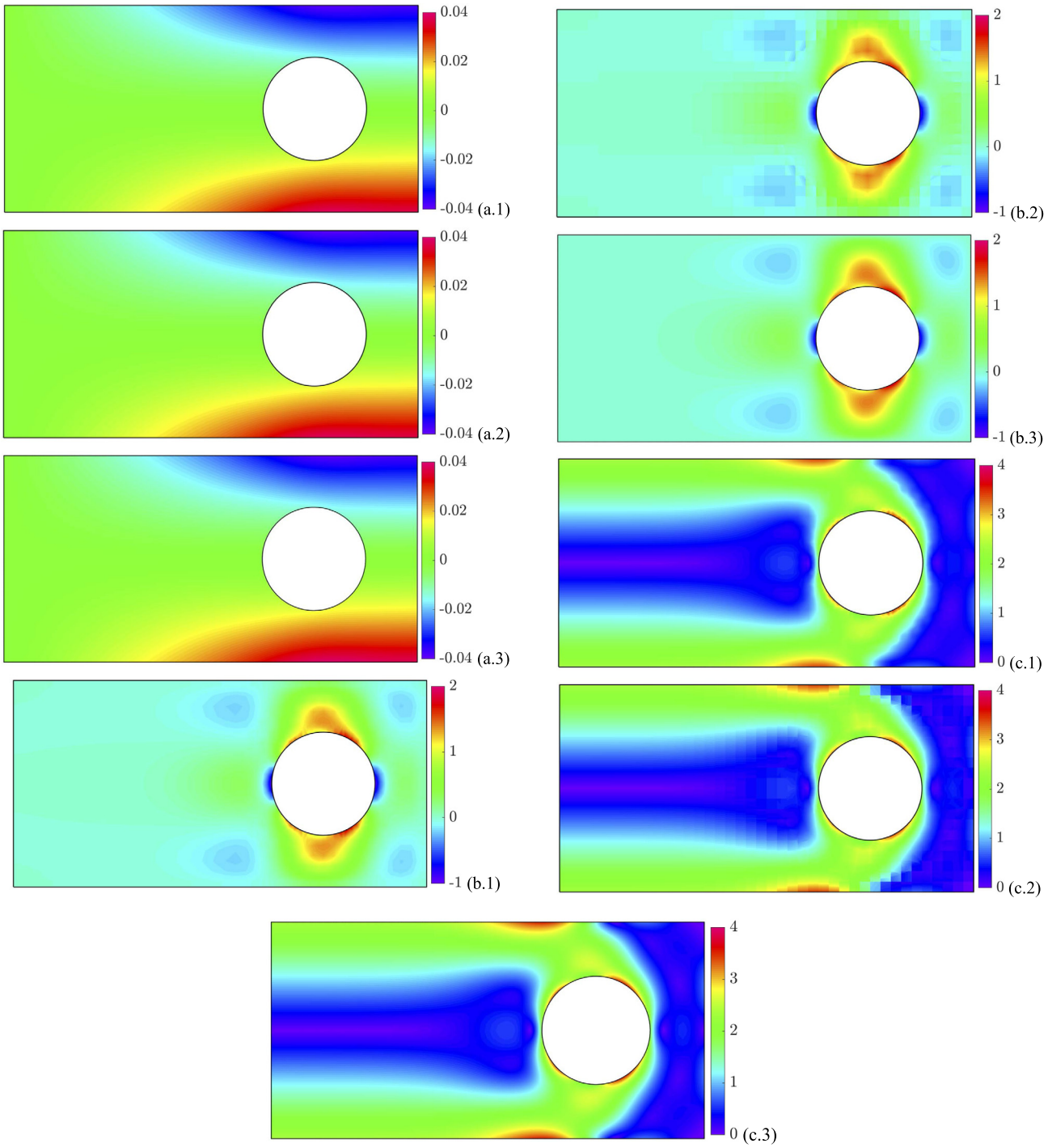

Fig. 5. (a.1) The numerical solution for the horizontal displacement using AMORE with overlapping elements. (a.2) The numerical solution for the horizontal displacement using AMORE with overlapping meshes. (a.3) The reference solution for the horizontal displacement. (b.1) The numerical solution (averaged) for the shear stress τ_{xy} using AMORE with overlapping elements. (b.2) The numerical solution (non-smoothed) for the shear stress τ_{xy} using AMORE with overlapping meshes. (b.3) The reference solution for the shear stress τ_{xy}. (c.1) The numerical solution (averaged) for the effective stress $\bar{\tau}$ using AMORE with overlapping elements. (c.2) The numerical solution (non-smoothed) for the effective stress $\bar{\tau}$ using AMORE with overlapping meshes. (c.3) The reference solution for the effective stress $\bar{\tau}$.

$$
\begin{aligned}
|u-u^*|^2_{1,\cup_i\Omega_{i,o}} &= \int_{\cup_i\Omega_{i,o}} \left\{ \left[\frac{\partial(u-u^*)}{\partial x}\right]^2 + \left[\frac{\partial(u-u^*)}{\partial y}\right]^2 \right\} \mathrm{d}\Omega \\
&= \int_{\cup_i\Omega_{i,o}} \left\{ \left[\frac{\partial \sum_i (w_i(u-u_i^*))}{\partial x}\right]^2 + \left[\frac{\partial \sum_i (w_i(u-u_i^*))}{\partial y}\right]^2 \right\} \mathrm{d}\Omega,
\end{aligned}
\tag{18}
$$

since $u = \sum_i w_i u$. We then have

$$
\begin{aligned}
\left[\frac{\partial \sum_i (w_i(u-u_i^*))}{\partial x}\right]^2 &= \left[\sum_i \frac{\partial w_i}{\partial x}(u-u_i^*) + \sum_i w_i \frac{\partial(u-u_i^*)}{\partial x}\right]^2 \\
&\leqslant \left[\sum_i \left|\frac{\partial w_i}{\partial x}(u-u_i^*)\right| + \sum_i \left|w_i \frac{\partial(u-u_i^*)}{\partial x}\right|\right]^2 \\
&\leqslant 2m \left[\sum_i \left|\frac{\partial w_i}{\partial x}(u-u_i^*)\right|^2 + \sum_i \left|w_i \frac{\partial(u-u_i^*)}{\partial x}\right|^2\right],
\end{aligned}
\tag{19}
$$

where the last inequality is due to the Cauchy-Schwarz inequality $\left(\sum_{i=1}^{n} a_i b_i\right)^2 \leqslant \left(\sum_{i=1}^{n} a_i^2\right)\left(\sum_{i=1}^{n} b_i^2\right)$ with $n = 2m$, $a_i = 1$ for $i = 1, \ldots, n$, $b_i = \left|\frac{\partial w_i}{\partial x}(u - u_i^*)\right|$ for $i = 1, \ldots, m$, and $b_{m+i} = \left|w_i \frac{\partial (u - u_i^*)}{\partial x}\right|$ for $i = 1, \ldots, m$. We note that the bound is not sharp because $a_i = \theta b_i$ is unlikely to hold for a constant θ. A similar result holds for $\left[\frac{\partial \sum_i (w_i (u - u_i^*))}{\partial y}\right]^2$.

Substituting these bounds into equation (18) and using (5) and (16) yields

$$
\begin{aligned}
|u - u^*|^2_{1,\cup_i \Omega_{i,o}} &\leqslant C \int_{\cup_i \Omega_{i,o}} \left\{ \sum_i \left(\chi_{\Omega_{i,o}} \frac{1}{\min\{h_i, h^*\}^2} |u - u_i^*|^2 \right) \right. \\
&\quad \left. + \sum_i \left[\chi_{\Omega_{i,o}} \left| \frac{\partial (u - u_i^*)}{\partial x} \right|^2 \right] + \sum_i \left[\chi_{\Omega_{i,o}} \left| \frac{\partial (u - u_i^*)}{\partial y} \right|^2 \right] \right\} \mathrm{d}\Omega \\
&\leqslant C \sum_i \left(\frac{1}{\min\{h_i, h^*\}^2} \| u - u_i^* \|^2_{0,\Omega_{i,o}} \right) + C \sum_i |u - u_i^*|^2_{1,\Omega_{i,o}} \\
&\leqslant C \sum_i \left(\frac{h_i^2}{\min\{h_i, h^*\}^2} h_i^{2k_i} \right) + C \sum_i h_i^{2k_i},
\end{aligned}
\tag{20}
$$

where $\chi_{\Omega_{i,o}}$ equals 1 on $\Omega_{i,o}$ and vanishes outside $\Omega_{i,o}$. If the overlapped regions are thick enough, i.e. $\gamma h_i \leqslant h^*$ for all i, where γ is a positive constant, we have $|u - u^*|^2_{1,\cup_i \Omega_{i,o}} \leqslant C \sum_i h_i^{2k_i}$. The total approximation error is then

$$
|u - u^*|^2_{1,\Omega} \leqslant C \sum_i h_i^{2k_i}. \tag{21}
$$

As expected, if all meshes have close element sizes, the global convergence rate is determined by finite elements of the lowest order.

4.4. A limit case of overlapping meshes

The error bound for overlapping meshes relies on the assumption that all overlapped regions are thick enough. The bound is not applicable if we let the overlapping size $h^* \to 0$ while keeping all h_i ($i = 1, \ldots, m$) finite. We are interested to see whether the solution converges in the limit case of $h^* \to 0$, and if an error bound independent of h^* can be established. Two numerical examples are studied for this purpose.

4.4.1. A thin beam problem

We solve the thin beam problem shown in Fig. 6(a). The reference solution of the deflection (using Timoshenko beam theory) at the free end is 0.1081. The two overlapping 9-node finite element meshes are shown in Fig. 6(b). The overlapping size is denoted by h^*.

As h^* tends to zero, we keep all elements at the constant length = 1 except for the leftmost red element which decreases in length. We would like that in the limit case, the numerical solution corresponds to the conforming mesh solution using six equal size 9-node elements. This is indeed the case as shown in Table 2, in which $h^* = 0$ represents the conforming mesh solutions with six equal elements.

4.4.2. A thick beam problem

We consider now a thick beam with more complicated overlapping meshes, as plotted in Fig. 7. By definition, the overlapping size $h^* = \min\{a, b\}$. The numerical solutions of the strain energy are listed in Table 3. The limit mesh is also solved using the gluing mesh feature in ADINA. The solution for the strain energy using the gluing mesh feature in ADINA [35] with $a = b = 0$ is 2.45995E + 01, and hence slightly different from the value given in Table 3 for the case $a = b = 0.0001$.

It can be seen that as $h^* = a = b \to 0.0001$, the energy solution does not increase monotonically. Indeed, we cannot expect monotonic convergence. Also, the energy solutions given in Table 3 are not symmetric with respect to a and b because the triangulation used for the numerical integration (see Section 3) was not symmetric. This emphasizes that further research is needed to establish more effective integration schemes [5].

4.4.3. Discussion

Although we realize that the solutions do not necessarily converge monotonically as the overlap decreases in size ($h^* \to 0.0001$), we observed that, at least for the two example problems, the solution difference is small when compared to a single mesh solution or a gluing mesh solution. Another important observation is that the condition number of the stiffness matrix obtained with a small overlapping size is very large, and increases rapidly as the overlapping size decreases. Therefore, it is best to use moderately thick overlapped regions.

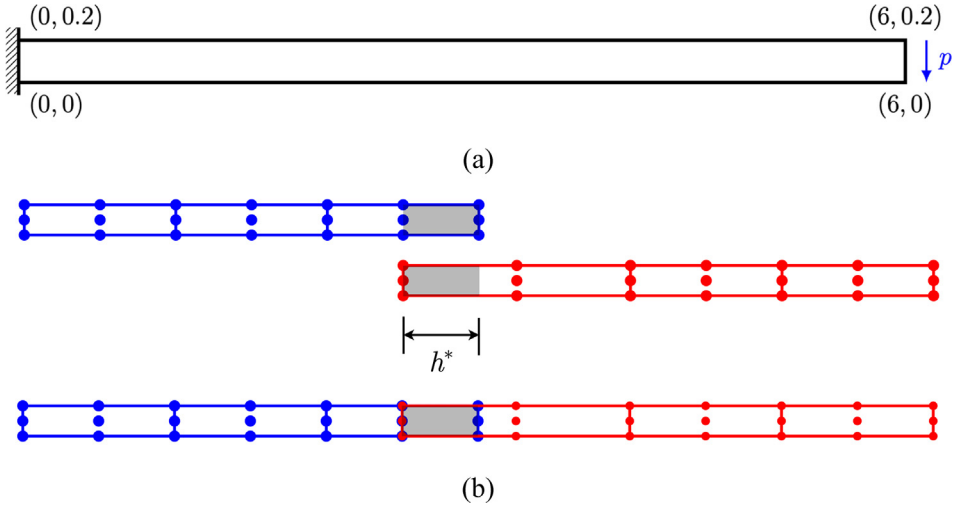

Fig. 6. (a) The thin beam problem: total applied force = 1, $E = 10^6$, $\nu = 0.3$, unit thickness, plane stress assumption. (b) The overlapping size h^*. All elements are of unit length except for the leftmost element in the red mesh. (For interpretation of the references to color in this figure legend, the reader is referred to the web version of this article.)

Table 2
Numerical solutions at different overlapping sizes h^*.

h^*	0.5	0.1	0.01
Tip deflection	0.106946	0.107049	0.107040
Energy	5.34726E−02	5.35241E−02	5.35194E−02
h^*	0.001	0.0001	0
Tip deflection	0.107035	0.107034	0.107034
Energy	5.35174E−02	5.35168E−02	5.35167E−02

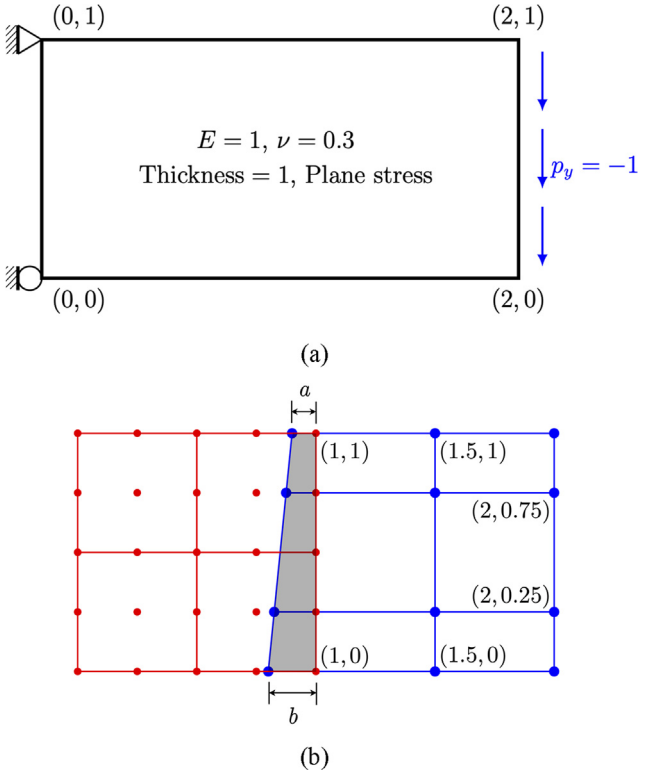

Fig. 7. (a) The thick beam. (b) A 9-node element mesh is overlapping a 4-node element mesh. The amount of overlapping is parametrized by a and b.

4.4.4. A one-dimensional case

We are able to show that in the one-dimensional case, the overlapping meshes yield an error bound independent of the overlapping size. This also partially explains the convergence results obtained in the solution of the thin beam problem, since the overlapping is essentially one-dimensional. The extension to special cases in two dimensions should not be difficult.

We consider the overlapping of a linear element and a quadratic element, as shown in Fig. 8(a). The weight functions are given in Fig. 8(b). The first-order derivatives of the weight functions satisfy

$$\left|\frac{dw_i}{dx}\right| = \frac{1}{h^*} \quad (i = 1, 2). \tag{22}$$

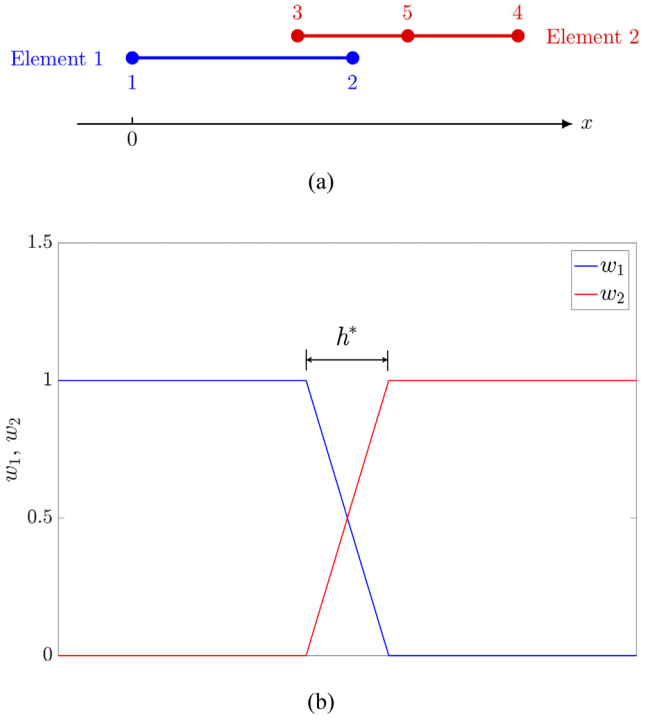

Fig. 8. (a) A linear element overlaps a quadratic element. (b) The weight functions.

We first introduce the classic interpolation results. Assume an unknown target function $f : [a, b] \to \mathbb{R}$ has derivatives up to the order $(k+1)$. If a polynomial interpolation P_k of order k satisfies $f(x_i) = P_k(x_i) \quad (i = 0, 1, \ldots, k)$ at the data points $a = x_0 < x_1 < \ldots < x_k = b$, then we have the error equation

$$f(x) - P_k(x) = f^{(k+1)}(\xi)\frac{w_{k+1}(x)}{(k+1)!}, \tag{23}$$

where $x \in [a, b]$, $w_{k+1}(x) = \Pi_{i=0}^{k}(x - x_i)$, ξ is a point in (a, b), and $f^{(k+1)}(\xi)$is the $k+1$st derivative of f at ξ. Clearly, $w_{k+1}(x_i) = 0$ and $f(x_i) = P_k(x_i)$ as expected. Assuming good boundedness on the derivative, and considering the upper bound for any ξ, the basic meaning of (23) is that the interpolation will differ from the unknown target function by a polynomial $w_{k+1}(x)$ which is zero at the known data points.

Such an interpolation necessarily yields $f'(y_i) = P_k'(y_i)$ with $y_i \in (x_{i-1}, x_i)$ $(i = 1, \ldots, k)$ due to Rolle's theorem in Calculus. Let $w_k^*(x) = \Pi_{i=1}^{k}(x - y_i)$. For any $x \in [a, b]$, using (23) we see there exists a point $\xi^* \in (a, b)$ such that

$$f'(x) - P_k'(x) = f^{(k+1)}(\xi^*)\frac{w_k^*(x)}{k!}. \tag{24}$$

We can now give the error bound for overlapping meshes in one dimension using the interpolation error equations (23) and (24). Assuming that the exact solution of our model problem has

Table 3
Numerical solutions of strain energy for different parameters (a, b).

b	a				
	0.2	0.1	0.01	0.001	0.0001
0.2	2.46632E+01	2.46658E+01	2.46530E+01	2.46269E+01	–
0.1	2.46779E+01	2.46891E+01	2.46877E+01	2.46692E+01	–
0.01	2.46844E+01	2.47027E+01	2.47020E+01	2.46839E+01	–
0.001	2.46672E+01	2.46904E+01	2.46863E+01	2.46484E+01	–
0.0001	–	–	–	–	2.45857E+01

bounded derivatives up to the third order we can find local approximations u_1^* (linear approximation on the first element) and u_2^* (quadratic approximation on the second element) such that we have the following pointwise error bounds

$$\begin{aligned} &|u-u_1^*| \leqslant Ch_1 h^*, \\ &|u-u_2^*| \leqslant Ch_2^2 h^*, \\ &\left|\tfrac{\mathrm{d}}{\mathrm{d}x}(u-u_1^*)\right| \leqslant Ch_1, \\ &\left|\tfrac{\mathrm{d}}{\mathrm{d}x}(u-u_2^*)\right| \leqslant Ch_2^2, \end{aligned} \tag{25}$$

for any point on the overlapped region, where h_i is the element size of the i-th element, and C is a generic constant. We also have on the overlapped region

$$|u_1^*-u_2^*| \leqslant C(h_1,h_2)h^*. \tag{26}$$

Taking the global approximation as $u^* = w_1u_1^* + w_2u_2^*$, the approximation error over the overlapped region is

$$|u-u^*|^2_{1,\Omega_1\cap\Omega_2} = \int_{\Omega_1\cap\Omega_2} \left|\frac{\mathrm{d}}{\mathrm{d}x}(u-u^*)\right|^2 \mathrm{d}x. \tag{27}$$

Since

$$\begin{aligned} \left|\tfrac{\mathrm{d}}{\mathrm{d}x}(u-u^*)\right| &= \left|\tfrac{\mathrm{d}}{\mathrm{d}x}\left[(w_1+w_2)(u-u_1^*)+w_2(u_1^*-u_2^*)\right]\right| \\ &= \left|\tfrac{\mathrm{d}}{\mathrm{d}x}\left[(u-u_1^*)+w_2(u_1^*-u_2^*)\right]\right| \\ &\leqslant \left|\tfrac{\mathrm{d}}{\mathrm{d}x}(u-u_1^*)\right| + \left|\tfrac{\mathrm{d}}{\mathrm{d}x}\left[w_2(u_1^*-u_2^*)\right]\right| \\ &\leqslant C(h_1,h_2), \end{aligned} \tag{28}$$

where we use $w_1+w_2=1$, equation (22) and the bounds (25) and (26), we see that the integrand in equation (27) is bounded. Therefore, the approximation error over the overlapped region tends to zero as the overlapping size decreases. A solution error independent of the overlapping size can then directly be obtained. The key is to show that we are able to find two local approximations that are close to each other on the overlapped region.

5. Concluding remarks

We reviewed two recently proposed finite element schemes for reducing the meshing effort in finite element analyses and showed how these schemes can be used in the AMORE paradigm to solve practical engineering problems. The overlapping elements combine advantages from both meshless methods and traditional finite element methods through a composite interpolation. The elements are insensitive to element distortions and have a good predictive capability. The method of overlapping meshes is based on a partition of unity formulation and efficient algorithms for computing weight functions and performing the numerical integration. Individual meshes may overlap freely and local enrichments can be conveniently imposed.

The overlapping elements give a convergence rate equal to the order of the polynomials used as degrees of freedom.

For the overlapping meshes, the global convergence rate is determined by the mesh with the lowest-order elements, provided that the overlapped regions are sufficiently thick. If an overlapped region decreases to be very small, the solution may still be acceptable, but the condition number of the stiffness matrix grows rapidly. Only for the simple one-dimensional case of overlapping meshes could we prove, based on classic interpolation theory, that the error bound is independent of the overlapping size. We thus suggest using overlapping meshes with moderately thick overlapped regions, at least of the magnitude of the smallest element size.

While only two-dimensional problems were solved in this paper, the theory given is also valuable for three-dimensional solutions. However, further research is needed for three-dimensional analysis, in particular to assess in detail the computational times required. Also, in all cases stress recovery techniques might be investigated and developed to increase the accuracy of the stress predictions.

Finally, it would be valuable to investigate the use of the overlapping elements and meshes in AMORE for general nonlinear analysis, dynamics, and multi-physics problems to reach the full potential of these schemes.

Declaration of Competing Interest

The authors declare that they have no known competing financial interests or personal relationships that could have appeared to influence the work reported in this paper.

References

[1] Bathe KJ. Finite element procedures. Prentice Hall; 1996. 2nd ed. KJ Bathe, Watertown, MA; 2014, and Higher Education Press, Beijing; 2016.
[2] Zhang L, Bathe KJ. Overlapping finite elements for a new paradigm of solution. Comput Struct 2017;187:64–76.
[3] Zhang L, Kim KT, Bathe KJ. The new paradigm of finite element solutions with overlapping elements in CAD – Computational efficiency of the procedure. Comput Struct 2018;199:1–17.
[4] Huang J, Bathe KJ. Quadrilateral overlapping elements and their use in the AMORE paradigm. Comput Struct 2019;222:25–35.
[5] Huang J, Bathe KJ. Overlapping finite element meshes in AMORE. Adv Eng Softw 2020;144:102791.
[6] De S, Bathe KJ. The method of finite spheres. Comput Mech 2000;25(4):329–45.
[7] Liu GR. Meshfree methods: moving beyond the finite element method. Taylor & Francis; 2009.
[8] de Berg M, Cheong O, van Kreveld M, Overmars M. Computational geometry: algorithms and applications. 3rd ed. Berlin Heidelberg: Springer-Verlag; 2008.
[9] Bentley JL, Ottmann TA. Algorithms for reporting and counting geometric intersections. IEEE Trans Comput 1979;C-28(9):643–7.
[10] Bathe KJ. The finite element method with "overlapping finite elements". In: Zingoni A, editor. Proceedings sixth international conference on structural engineering, mechanics and computation – SEMC 2016, Cape Town, South Africa; 2016.
[11] Bathe KJ. The AMORE paradigm for finite element analysis. Adv Eng Softw 2019;130:1–13.
[12] Bathe KJ, Zhang L. The finite element method with overlapping elements – A new paradigm for CAD driven simulations. Comput Struct 2017;182:526–39.
[13] Chesshire G, Henshaw WD. Composite overlapping meshes for the solution of partial differential equations. J Comput Phys 1990;90(1):1–64.
[14] Steger JL, Benek JA. On the use of composite grid schemes in computational aerodynamics. Comput Methods Appl Mech Eng 1987;64(1–3):301–20.
[15] Benek JA, Buning PG, Steger JL. A 3-D Chimera grid embedding technique. In: 7th Computational Physics Conference, Cincinnati, USA; 1985.
[16] Strouboulis T, Copps K, Babuška I. The generalized finite element method. Comput Methods Appl Mech Eng 2001;190(32–33):4081–193.
[17] Strouboulis T, Babuška I, Copps K. The design and analysis of the generalized finite element method. Comput Methods Appl Mech Eng 2000;181(1–3):43–69.
[18] Duarte CA, Babuška I, Oden JT. Generalized finite element methods for three-dimensional structural mechanics problems. Comput Struct 2000;77(2):215–32.
[19] Glowinski R, Pan T-W, Hesla TI, Joseph DD. A distributed Lagrange multiplier/fictitious domain method for particulate flows. Int J Multiph Flow 1999;25(5):755–94.
[20] Glowinski R, Pan T-W, Periaux J. A fictitious domain method for Dirichlet problem and applications. Comput Methods Appl Mech Eng 1994;111(3–4):283–303.
[21] Dolean V, Jolivet P, Nataf F. An introduction to domain decomposition methods: Algorithms, theory and parallel implementation. SIAM 2015.
[22] Hansbo A, Hansbo P, Larson M. A finite element method on composite grids based on Nitsche's method. ESAIM: Math Model Numer Anal 2003;37(3):495–514.
[23] Massing A, Larson MG, Logg A. Efficient implementation of finite element methods on nonmatching and overlapping meshes in three dimensions. SIAM J Sci Comput 2013;35(1):C23–47.
[24] Brezzi F, Manzini G, Marini D, Pietra RA, Russo A. Discontinuous Galerkin approximations for elliptic problems. Numer Methods Partial Differ Equ 2000;16(4):365–78.
[25] Arnold DN, Brezzi F, Cockburn B, Marini LD. Unified analysis of discontinuous Galerkin methods for elliptic problems. SIAM J Numer Anal 2002;39(5):1749–79.
[26] Kim KT, Zhang L, Bathe KJ. Transient implicit wave propagation dynamics with overlapping finite elements. Comput Struct 2018;199:18–33.

[27] Chai Y, Bathe KJ. Transient wave propagation in inhomogeneous media with enriched overlapping triangular elements. Comput Struct 2020;237:106273.
[28] Ibrahimbegovic A, Wilson EL. A modified method of incompatible modes. Commun Appl Numer Methods 1991;7(3):187–94.
[29] Payen DJ, Bathe KJ. A stress improvement procedure. Comput Struct 2012;112–113:311–26.
[30] Duvaut G, Lions JL. Inequalities in Mechanics and Physics. Springer-Verlag, Berlin Heidelberg; 1976. Translated from the French by CW John.
[31] Ciarlet PG. The finite element method for elliptic problems. SIAM 2002.
[32] Chen Z, Wu H. Selected topics in finite element methods. Beijing: Science Press; 2010.
[33] Chapelle D, Bathe KJ. The finite element analysis of shells – Fundamentals. 2nd ed. Springer; 2011.
[34] Ciarlet PG, Raviart P-A. Interpolation theory over curved elements, with applications to finite element methods. Comput Methods Appl Mech Eng 1972;1(2):217–49.
[35] ADINA R&D, Inc. ADINA theory and modeling guide. Volume I: ADINA solids & structures. ADINA R&D, Inc., MA; 2019.